Experimental quantum-information processing with $^{43}Ca^{+}$ ions

J. Benhelm,[1,2] G. Kirchmair,[1,2] C. F. Roos,[1,2] and R. Blatt[1,2]
[1]*Institut für Experimentalphysik, Universität Innsbruck, Technikerstrasse 25, A-6020 Innsbruck, Austria*
[2]*Institut für Quantenoptik und Quanteninformation, Österreichische Akademie der Wissenschaften, Otto-Hittmair-Platz 1, A-6020 Innsbruck, Austria*

(Received 8 April 2008; published 4 June 2008)

For quantum-information processing (QIP) with trapped ions, the isotope $^{43}Ca^{+}$ offers the combined advantages of a quantum memory with long coherence time, a high-fidelity readout, and the possibility of performing two-qubit gates on a quadrupole transition with a narrow-band laser. Compared to other ions used for quantum computing, $^{43}Ca^{+}$ has a relatively complicated level structure. We discuss how to meet the basic requirements for QIP and demonstrate ground-state cooling, robust state initialization, and efficient readout for the hyperfine qubit with a single $^{43}Ca^{+}$ ion. A microwave field and a Raman light field are used to drive qubit transitions, and the coherence times for both fields are compared. Phase errors due to interferometric instabilities in the Raman field generation do not limit the experiments on a time scale of 100 ms. We find a quantum-information storage time of many seconds for the hyperfine qubit.

DOI: 10.1103/PhysRevA.77.062306 PACS number(s): 03.67.Lx, 32.80.Qk, 37.10.Ty, 42.50.Dv

I. INTRODUCTION

Quantum-information processing (QIP) with trapped ions has made huge progress since it was first proposed more than a decade ago [1]. The question of which ion species is best suited for QIP is still undecided. So far, qubits encoded in trapped ions come in two flavors. On the one hand, two energy levels of the hyperfine (or Zeeman) ground-state manifold of an ion can serve as a qubit commonly termed a *hyperfine qubit*. The energy splitting is typically several GHz. Many successful experiments have been performed on hyperfine qubits with cadmium and beryllium ions, illustrating the capabilities for QIP [2–5]. On the other hand, quantum information can be encoded in the ground state and a metastable energy state of an ion. Here the energy splitting lies in the optical domain and the qubit is therefore referred to as an *optical qubit*. This concept has been pursued so far mainly with calcium ions, where all major building blocks for QIP have been demonstrated [6–8].

When it comes to judging the suitability of a particular ion for QIP, the fidelities and speed of the basic gate operations and the quantum-information storage time are important criteria. Concerning the latter the hyperfine qubit has been the clearly better choice. For the optical qubit, it is technically challenging to achieve quantum-information storage times much longer than a few milliseconds since this requires a laser with a linewidth of less than a few Hz. Yet optical qubits have excellent initialization and readout properties. Moreover, the metastable states can be used as intermediate levels when driving the hyperfine qubits with a Raman light field as suggested in Ref. [9]. Errors induced by spontaneous scattering, which are a major limitation in present experiments with Raman light fields detuned from an optical dipole transition, are then largely suppressed.

From today's perspective, it seems necessary to integrate the building blocks that have been acquired over the years into a single system. By using hyperfine qubits in combination with metastable states, it is possible to exploit the best of both concepts. Only a few ion species offer this possibility, one of them being $^{43}Ca^{+}$. It is the only calcium isotope with nonzero nuclear spin, and it offers the advantage that all necessary laser wavelengths lying within the range from 375 nm to 866 nm can be produced by commercially available solid-state lasers. For QIP, only a small number of electronic levels are of interest (Fig. 1). The $S_{1/2}$ ground state is split into the states $F=4$ and $F=3$ with a hyperfine splitting of 3.2

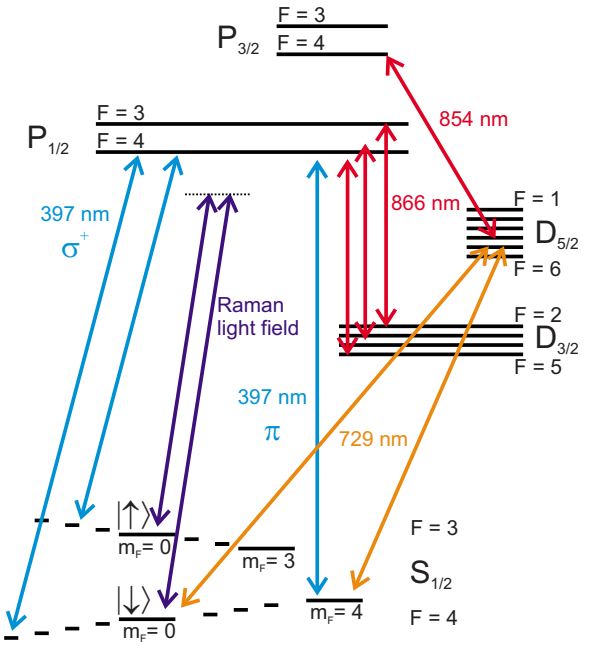

FIG. 1. (Color online) Energy level diagram of the valence electron of $^{43}Ca^{+}$ showing the hyperfine splitting of the lowest energy levels. Laser light at 397 nm is used for Doppler cooling and detection; the lasers at 866 nm and 854 nm pump out the metastable D states. A laser at 729 nm excites the ions on the transition from the $S_{1/2}(F=4)$ states to the $D_{5/2}(F=2,\ldots,6)$ states. It is used for ground-state cooling, state initialization, and state discrimination. Microwave radiation applied to an electrode close to the ions as well as a Raman light field at 397 nm can drive transitions between different levels in the hyperfine structure of the $S_{1/2}$-state manifold.

GHz [10]. It is connected by electric-dipole transitions to the short-lived levels $P_{1/2}$ and $P_{3/2}$ and by electric-quadrupole transitions to the metastable states $D_{3/2}$ and $D_{5/2}$ with a lifetime of ~ 1 s. Because of the fairly large nuclear spin of $I=7/2$, these levels split into a total of 144 Zeeman states. This results in a very rich spectrum for the $S_{1/2} \leftrightarrow D_{5/2}$ transition, which has been investigated to a high precision recently [11].

II. EXPERIMENTAL SETUP

$^{43}Ca^+$ ions are loaded from an enriched source into a linear Paul trap by a two-step photoionization process (423 nm and 375 nm) [11–13]. Radial confinement is provided by a quadrupole field created by the application of a radio frequency voltage to two out of four blade electrodes and connecting the other two blade electrodes to ground [14]. Axial confinement is achieved by setting two tip electrodes to dc voltages of 500–500 V, resulting in center-of-mass (c.m.) mode secular trapping frequencies of $\omega_{ax}/2\pi = 0.8-1.5$ MHz. Applying slightly unequal voltages to the tips leads to an axial shift in the ions' equilibrium position. The closest distance between the ions and the tip (blade) electrodes is 2.5 mm (0.8 mm). Two additional electrodes compensate for external electric stray fields in the radial directions. One of them, located at a distance of 7.3 mm to the trap center, can also be used to guide microwave signals to the ions. The trap is housed in a vacuum environment with a pressure below 2×10^{-11} mbar. When no laser light is present, ion storage times as long as 2 weeks have been observed.[1]

For most experimental steps, we use a titanium-sapphire laser at 729 nm for coupling the energy levels of the $S_{1/2}(F=4)$ and $D_{5/2}(F=2,\ldots,6)$ manifolds via their electric-quadrupole transition (Fig. 1). The laser's frequency is stabilized to an ultrastable Fabry-Perot cavity [15] with a linewidth of 4.7 kHz. A Lorentzian fit to a beat note measurement with another similar laser reveals a width of the beat note's power spectral density of 1.8 Hz (4 s data acquisition time). This is indicative of a linewidth for each laser below 1 Hz. In a measurement where a single $^{43}Ca^+$ ion served as a frequency reference [11], we obtained a linewidth of 16 Hz with an integration time of 60 s.

In order to stabilize the laser's frequency to the atomic transition frequency, we use a feedback loop based on spectroscopic measurements typically taken every 1–2 min. Since Ramsey phase experiments are used to probe the frequencies of two different Zeeman transitions, these measurements serve also to infer the strength of the magnetic field at the ion's position. The result is automatically analyzed and fed back to an acousto-optic modulator (AOM) located between the laser and its reference cavity. By this means the laser's output frequency remains constant with respect to the ion's quadrupole transition frequency. The mean frequency deviation between laser and ion depends on the Ramsey probe time, the measurement interval, and the actual frequency drift of the reference cavity and is typically smaller than 200 Hz. With the knowledge of the laser frequency and the magnetic field, the transition frequency of all required Zeeman transitions are calculated to an accuracy of ± 500 Hz. The optical frequency and phase of the laser are controlled with a double-pass AOM (270 MHz) between laser and ion. Slow drifts of the magnetic field ($\lesssim 200$ μG/h) are taken into account by properly adjusting the radio frequency feeding the AOM. Deteriorating effects due to magnetic field noise components at 50 Hz, typically on the order of 1 mG, are largely suppressed by triggering all experiments to the ac-line frequency.

The hyperfine qubit can be driven with a Raman light field comprising two phase stable frequency components. It is derived from a commercial diode laser system, consisting of a tapered amplifier and a frequency-doubling stage emitting at a wavelength of 397 nm. To achieve the frequency difference of 3.2 GHz required for bridging the ground-state hyperfine splitting in $^{43}Ca^+$, the light is first sent through an AOM (1 GHz) that splits the laser beam into a blue beam line (+1st order of diffraction) and a red beam line (0th order). The latter passes another AOM operated at 1 GHz (−1st order of diffraction). The remaining frequency shift is achieved by two more AOMs (~ 300 MHz) in each beamline. For noncopropagating Raman light fields, the two beam lines are separately guided to the ions through the viewports labeled NW and NE in Fig. 2(a).

Frequency, phase, and amplitude control of these lasers is synonymous to controlling the radio frequency signals applied to the AOMs. We use a homemade versatile frequency source (VFS) based on direct digital synthesis that can phase-coherently provide 16 different radio frequencies up to 305 MHz. Amplitude shaping is achieved with a variable-gain amplifier controlled by a field-programmable gate array. The VFS and all other radio frequency sources providing the input signals of the AOMs mentioned above are referenced to an ultrastable quartz oscillator with a long-term stabilization provided by the global positioning system. For direct microwave driving the hyperfine qubit, the output of the VFS is mixed with a signal of 1.35 GHz, then filtered, frequency doubled, filtered, and amplified. In this way, full amplitude, frequency, and phase control of the VFS is up-converted to 3.2 GHz.

The laser sources at 866 nm, 854 nm, and 397 nm are commercially available diode lasers whose frequencies are referenced to Fabry-Perot cavities. The Doppler cooling laser at 397 nm is produced by frequency-doubling light of a near-infrared laser diode. Except for the Raman light fields, all other light sources are linked to the experiment with single-mode fibers. As sketched in Fig. 2, the vacuum vessel provides optical access for illuminating the ion by laser beams mostly arriving in a plane containing also the symmetry axis of the trap. In addition, two beams used for laser cooling (729 nm and 866 nm) are sent in from below with a 60° angle to the trap axis.

Fluorescence light is collected with a custom-designed lens (with a numerical aperture of 0.3), correcting for aberrations induced by the vacuum window. The light is sent to a photomultiplier (PMT) or a sensitive camera with a magni-

[1]With two $^{40}Ca^+$ ions trapped, we repeatedly observe that one of the ions forms a $CaOH^+$ molecule by measuring the change of the axial sideband frequencies. These events occur every few hours.

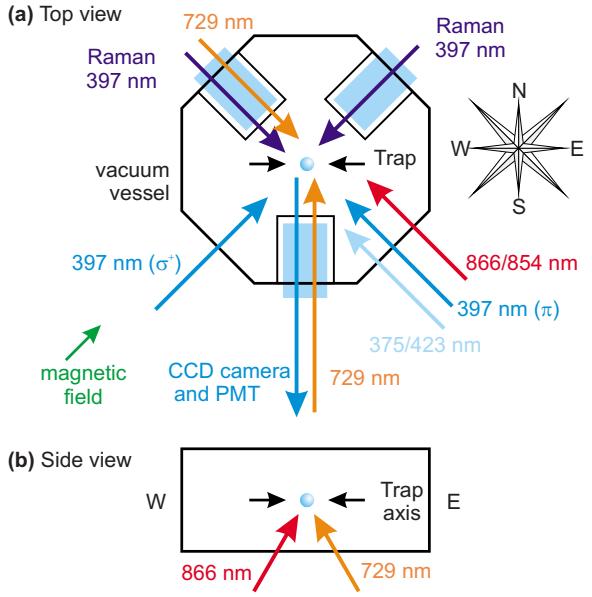

FIG. 2. (Color online) (a) Most laser beams are sent to the ion from a plane containing also the symmetry axis of the trap (top view). With three custom-made lenses in the inverted viewports S, NE, and NW, we can tightly focus light at wavelengths 729 nm and 397 nm. The lens in S is also used to collect fluorescence light which is sent to a PMT or a camera. The quantization axis is defined by a magnetic field along SW-NE. (b) Two beams (729 nm and 866 nm) are sent in from below in a 60° angle to the trap axis (side view). The axial trapping potential is provided by two tips indicated by arrows along the z axis. Unbalancing the tip voltages results in a shift of the ion crystal along the trap axis (E-W).

fication of 25 and a resolution of 2.2 μm. For a single $^{43}Ca^{+}$ ion, the signal-to-noise ratio at the PMT is typically around 50. The same type of lens is also used to focus light at 729 nm and 397 nm from the S, NE, and NW viewports.

III. INITIALIZING THE $^{43}Ca^{+}$ HYPERFINE QUBIT

There are many ways to encode quantum information in the $^{43}Ca^{+}$ level structure. An optical qubit with vanishing first-order dependence on magnetic field fluctuations has been proposed in Ref. [11]. Here, we consider the hyperfine ground-state manifold depicted in Fig. 1 where the energy splitting between the $F=3$ and $F=4$ manifold is about 3.2 GHz. For low magnetic fields, the two states $|\downarrow\rangle \equiv S_{1/2}(F=4,\ m_F=0)$ and $|\uparrow\rangle \equiv S_{1/2}(F=3,\ m_F=0)$ exhibit no linear Zeeman effect and are therefore attractive as a robust quantum-information carrier [16]. As in classical computing, QIP devices also need to be initialized. In our experiment, the initialization step comprises Doppler cooling, optical pumping, cooling to the motional ground state, and state transfer to $|\downarrow\rangle$.

A. Doppler cooling and optical pumping

For Doppler cooling and fluorescence detection, the ion is excited on the $S_{1/2} \leftrightarrow P_{1/2}$ dipole transition with two laser beams. The beam entering from SE is π polarized and is slightly red detuned from the transition $S_{1/2}(F=4) \leftrightarrow P_{1/2}(F=4)$. The second beam is σ^{+} polarized. It is sent through an electro-optic phase modulator (3.2 GHz) to excite the ions from the $S_{1/2}(F=3)$ and $S_{1/2}(F=4)$ to $P_{1/2}(F=4)$ manifold. Coherent population trapping is avoided by lifting the degeneracy of the Zeeman sublevels with a magnetic field. To avoid population trapping in the $D_{3/2}$ manifold, repumping laser light at 866 nm is applied. The repumping efficiency was improved by tuning the laser close to the $D_{3/2}(F=3) \leftrightarrow P_{1/2}(F=3)$ transition frequency and providing two additional frequencies shifted by −150 MHz and −395 MHz such that all hyperfine $D_{3/2}$ levels are resonantly coupled to one of the $P_{1/2}(F=3,4)$-levels. We observed a maximum fluorescence count rate of 24000 counts per second and per $^{43}Ca^{+}$ ion on a PMT for magnetic fields ranging from 0.2 to 5 G. This is about 45% of the count rate we observe for $^{40}Ca^{+}$ ions. The count rate difference, possibly caused by coherent population trapping, is still under investigation.

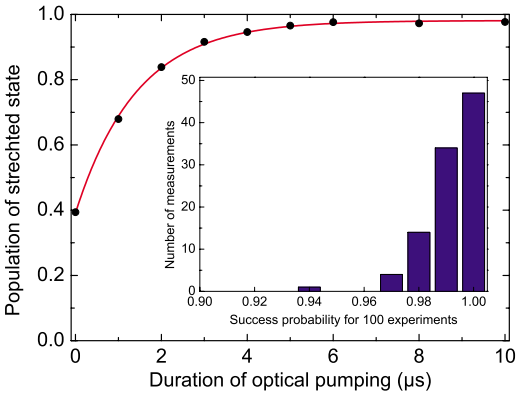

FIG. 3. (Color online) The population in the stretched state $S_{1/2}(F=4,\ m_F=4)$ is plotted as a function of the duration of optical pumping. An exponential fit (solid line) reveals a time constant of 1.4 μs. After 10 μs the population is in the desired state in 98% of the measurements. The inset shows a histogram of the success rate of 100 measurements each containing 100 experiments when two π pulses on the quadrupole transition are applied and an additional intermediated optical pumping interval is used. This enhances the fidelity of the process to above 99.2%.

After switching off the π-polarized laser beam, the ion is optically pumped into the state $S_{1/2}(F=4,\ m_F=4)$. The state's population was measured with two consecutive π pulses exciting the population to the $D_{5/2}$ state and subsequent fluorescence detection (Sec. IV). Figure 3 shows the dynamics of optical pumping and illustrates that the stretched Zeeman states of the ground-state manifold are already strongly populated during Doppler cooling. An exponential fit to the data points yields a time constant of the process of 1.4 μs. After 10 μs, the desired state is populated in 98% of the cases.

The pumping efficiency can be improved by transferring the population after this first step with a π pulse to the $D_{5/2}(F=6,\ m_F=6)$ state and repeating the optical pumping. By applying another π pulse on the same transition, the populations in $S_{1/2}(F=4,\ m_F=4)$ and $D_{5/2}(F=6,\ m_F=6)$ are exchanged. On average, 98% should now be in $S_{1/2}(F=4,\ m_F=4)$ and the rest in the $D_{5/2}$ state. Finally the two populations are combined by switching on the 854-nm laser

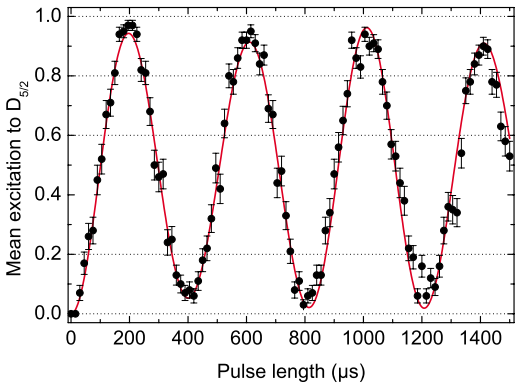

FIG. 4. (Color online) Rabi oscillations on the blue axial sideband of the transition $S_{1/2}(F=4,\ m_F=4) \leftrightarrow D_{5/2}(F=6,\ m_F=6)$ after ground-state cooling. The solid line is a fit assuming a thermal state. It yields a mean occupation of the axial mode of $\bar{n}_{ax}=0.06$.

for a short time to clear out the $D_{5/2}$ state via the $P_{3/2}(F=5,\ m_F=5)$ state from where it can decay only into the desired stretched state. The inset of Fig. 3 shows a histogram built from 100 measurements, each comprising 100 experiments, indicating a lower bound of the pumping efficiency of 99.2%.

After Doppler cooling and optical pumping, an average population $\bar{n}_{ax}=10(5)$ of the axial mode is inferred from measuring the decay of Rabi oscillations on the blue axial sideband. The average number of quanta is heavily dependent on the different laser detunings and powers.

B. Ground-state cooling, heating rate, and ion shuttling

Cooling the ions to the motional ground state is mandatory in order to maximize quantum gate fidelities. In our experiment, it has been implemented with a scheme analogous to what has been demonstrated with $^{40}Ca^+$ ions [17]. In order to obtain a closed cooling cycle, the frequency of the laser at 729 nm is tuned to the red sideband $(\omega_{ax}/2\pi=1.18$ MHz) of the transition $S_{1/2}(F=4,\ m_F=4) \leftrightarrow D_{5/2}(F=6,\ m_F=6)$. An additional quenching laser at 854 nm is required to increase the spontaneous decay rate to the energy level $S_{1/2}$ by coupling the $D_{5/2}(F=6,\ m_F=6)$ to the $P_{3/2}(F=5,\ m_F=5)$ state. Spontaneous decay to the stretched state takes the entropy away from the ion. In each cycle, one motional quantum can be removed. The residual occupation of the motional mode is measured by comparison of the red and blue sideband excitations. Alternatively, Rabi oscillations on a blue motional sideband can be observed in order to infer the average population of the axial mode (see Fig. 4). The solid line is a fitted model function with $\bar{n}_{ax}$ as a free parameter. From both methods, we consistently obtain $\bar{n}_{ax}=0.06$.

By introducing and varying a delay time between ground-state cooling and the temperature measurement, we determined a heating rate on the axial com-mode of 1 motional quantum per 370 ms. The coherence of a motional superposition state $|0\rangle+|1\rangle$ was investigated by performing Ramsey experiments that mapped the motional superposition states after a variable waiting time to the $S_{1/2}$ and $D_{5/2}$ electronic states. These measurements showed that the motional coherence was preserved for more than 320(10) ms, in good agreement with the measured heating rate.

When it comes to scaling the system up to strings of many ions, it is important that single-qubit gates can be applied to each individual ion. Individual addressing can be achieved by using an electro-optical deflector to rapidly steer a strongly focused laser beam to different ions in the string with high precision [14]. Driving Raman transitions in $^{43}Ca^+$ requires more than a single laser beam that would have to be steered this way. To avoid this complication, we prefer to shuttle the ion string along the axis of the trap instead of moving the laser beams. For an axial trapping frequency of $\omega_{ax}/(2\pi)=1.18$ MHz we are able to shuttle the ions over a distance of up to 10 μm by changing the right (left) tip voltage from 990 V (1010 V) to 1010 V (990 V). The switching speed is currently limited by a low-pass filter with a cutoff at 125 kHz, which prevents external electrical noise from coupling to the trap electrodes. Shuttling over the full distance in order to individually address single ions works for transport durations as low as 40 μs. In a test run with a single $^{40}Ca^+$ ion, quantum information encoded into the motional states $|n=0\rangle$ and $|n=1\rangle$ was fully preserved during the shuttling.

C. Transfer to the hyperfine clock states

Ground-state cooling on quadrupole transitions requires a closed cooling cycle which can only be achieved efficiently when working with the stretched hyperfine ground states $(F=4,\ m_F=\pm 4)$. For this reason, methods are needed that allow for a transfer from these states to the qubit state $|\downarrow\rangle$. Four different techniques were under consideration.

1. Optical pumping on the $S_{1/2}$ to $P_{1/2}$ transition

The state $|\downarrow\rangle$ could be populated by optical pumping with π-polarized light fields exciting the transitions $S_{1/2}(F=4) \leftrightarrow P_{1/2}(F=4)$ and $S_{1/2}(F=3) \leftrightarrow P_{1/2}(F=4)$ within a few microseconds. However, many scattering events would be required to pump the population to the desired state that are likely to heat up the ion from the motional ground state. Moreover, the efficiency of the optical pumping would probably be fairly poor as small polarization imperfections of the beams and repumping via the $S_{1/2}(F=4) \leftrightarrow P_{1/2}(F=3)$ are likely to occur.

2. Raman light field

Transferring the population can also be achieved with a Raman light field detuned from the $S_{1/2} \leftrightarrow P_{1/2}$ dipole transition at 397 nm. In the simplest scenario, a sequence of four π pulses would be used to populate the state $|\downarrow\rangle$ starting from $S_{1/2}(F=4,\ m_F=\pm 4)$ by changing the magnetic quantum number in units of $\Delta m=\pm 1$. Use of copropagating beams suppresses unwanted excitations of motional sidebands.

3. Microwave

Instead of a Raman light field, also a microwave field can be used to transfer the ions in a four-step process to $|\downarrow\rangle$. An additional advantage here is that the field's wavelength is

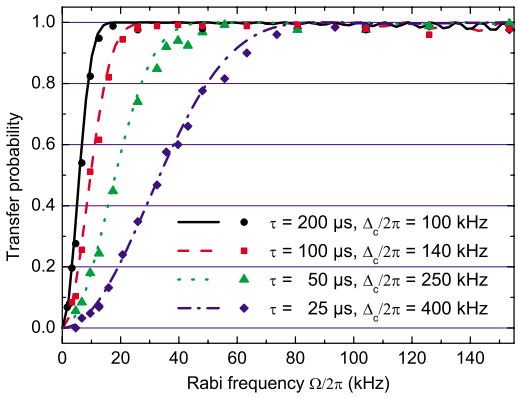

FIG. 5. (Color online) Transfer probability measurement of an amplitude shaped laser pulse on the transition $S_{1/2}(m_F=1/2) \leftrightarrow D_{5/2}(m_F=3/2)$ of a single $^{40}Ca^+$ ion as a function of the Rabi frequency. Data were taken for four different pulse lengths τ and frequency chirp spans Δ_c as given in the plot legend. The lines indicate what is theoretically expected. With enough laser power available, the transfer probability hardly changes over a wide range of Rabi frequencies.

huge compared to the distance of the ions and therefore an equal coupling of all ions to the field is guaranteed.

A limitation for both methods—Raman light field and microwave—is the small coupling strength on the transitions $(F=3,\ m_F=\pm 3) \leftrightarrow (F=4,\ m_F=\pm 2)$. That makes the whole process either slow or necessitates a larger frequency separation of the Zeeman levels in order to suppress nonresonant excitation of neighboring transitions.

4. Transfer via quadrupole transitions

State transfer based on a laser operating on the quadrupole transition $S_{1/2} \leftrightarrow D_{5/2}$ reduces the transfer process to two steps since the selection rules allow for $\Delta m = \pm 2$. The duration of a π pulse can be as short as a few microseconds, and only a single laser beam is needed that can be either focused to a small region or illuminate the whole trap volume. If the $D_{5/2}(F=4)$ is chosen as intermediate state, a good compromise is achieved between the quadrupole coupling strength of the involved transitions and the frequency separation of the neighboring D-state Zeeman levels. The latter is by a factor 1.6 larger as for the ground states. In particular, for low magnetic fields this method is expected to work better than a transfer with Raman or microwave fields.

With the precision laser for the quadrupole transition acting on a single $^{43}Ca^+$ ion, the implementation of state transfer is straightforward. With two consecutive π pulses, we achieved a transfer success probability of more than 99%. Assuming Gaussian beam waists, such high probabilities cannot be expected for larger ions crystals though, unless one is willing to waste most of the laser power by making the beam size very large. As variations of the coupling strengths may also arise from other technical imperfections, a more robust scheme seems to be desirable. Inspired by Ref. [18], we introduce amplitude shaping and a linear frequency sweep of the transfer pulses to demonstrate a transfer technique less sensitive to changes in the laser intensity. Figure 5 shows the transfer probability for a single $^{40}Ca^+$ ion and the transition $S_{1/2}(m=1/2) \leftrightarrow D_{5/2}(m=3/2)$ as a function of the Rabi frequency for four different pulse durations τ. The amplitude of the laser pulse had a $\cos^2$ shape over the pulse length. The frequency of the laser was linearly swept over a range Δ_c centered on the transition frequency. The data show clearly that the transfer probability is hardly affected over a broad range of Rabi frequencies Ω for the different parameters.

IV. STATE DETECTION

For $^{43}Ca^+$ ions, the electron shelving technique first introduced by Dehmelt [21] allows for an efficient state discrimination between the $|\downarrow\rangle$ and $|\uparrow\rangle$ hyperfine qubit states by scattering light on the $S_{1/2}$ to $P_{1/2}$ transition after having shelved the $|\downarrow\rangle$ state in the $D_{5/2}$ metastable state with a π pulse. In our experiment, the same light fields as for Doppler cooling are used, but with slightly more power. With this method, not only $|\uparrow\rangle$ and $|\downarrow\rangle$ can be discriminated, but the other Zeeman levels in the $S_{1/2}$-state and $D_{5/2}$-state manifolds, too. The quality of the transfer pulses sets a limitation on the state discrimination. Again, pulse shaping and frequency sweeping can help to increase the robustness with respect to intensity variations of the shelving laser. In addition, instead of using a single π-pulse excitation to a certain Zeeman state in the $D_{5/2}$-state manifold, the first π pulse can be followed by a second one, exciting any population still remaining in $|\downarrow\rangle$ to a different Zeeman state. Assuming a transfer probability of 0.99 for each of the pulses, one expects a transfer error probability of less then 10^{-4}. The final detection fidelity will then be limited by spontaneous decay from the $D_{5/2}$ state during the detection whose duration depends on the signal-to-noise ratio and signal strength. For the experiments reported here, the detection time was set to 5 ms. The error due to spontaneous decay is estimated to be 0.5%.

V. SINGLE-QUBIT GATES ON THE $^{43}Ca^+$ HYPERFINE QUBIT

Once external and internal degrees of freedom are initialized, quantum information needs to be encoded into the ions, stored, and manipulated. This is achieved with a driving field tuned to the qubits' transition frequency. Two different driving fields were investigated.

A. Microwave drive

From an experimental point of view, quantum-state manipulation by microwave radiation is simple and robust. There is no alignment required, and stable frequency sources are readily available with computer-controlled power, frequency, and phase.

To characterize the microwave properties on a single $^{43}Ca^+$ ion, Rabi oscillations were recorded on the hyperfine qubit $|\downarrow\rangle \leftrightarrow |\uparrow\rangle$ at a magnetic field of 3.4 G. After initializing the ion into $|\downarrow\rangle$, a microwave signal of 3.226 GHz is turned on for a variable amount of time followed by state detection. Figure 6 shows the resulting Rabi oscillations at instances of

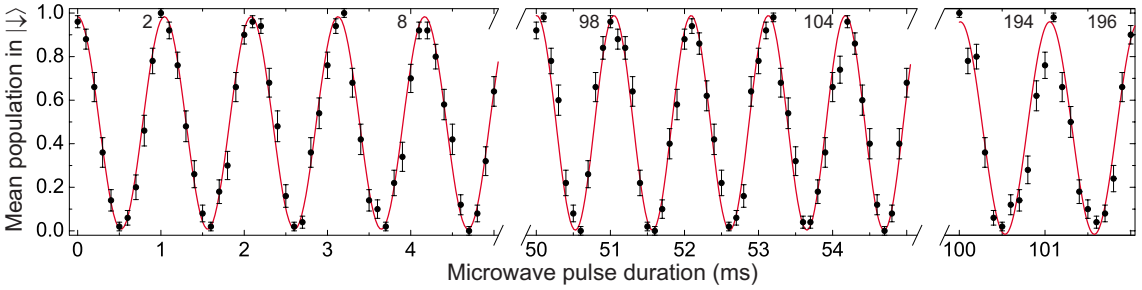

FIG. 6. (Color online) Rabi oscillations on the $^{43}Ca^{+}$ hyperfine qubit mediated by a microwave field after 0, 50, and 100 ms. Each data point represent 50 individual measurements. The solid line is a weighted least-squares fit with the function $\frac{A}{2}\cos(\pi t/\tau_\pi)+y_0$, resulting in $y_0=0.490(3)$, $\tau_\pi=520.83(3)$ μs, and $A=0.974(11)$. The number of state transfers is indicated. Since the amplitude of the Rabi oscillation is still close to unity even after 200 state transfers, the microwave can serve as a reference to the Raman light field regarding power and phase stability.

0, 50, and 100 ms. The solid line represents a weighted least-squares fit to the function $f(t)=\frac{A}{2}\cos(\pi t/\tau_\pi)+y_0$, resulting in $y_0=0.490(3)$, $\tau_\pi=520.83(3)$ μs, and $A=0.974(11)$. About 200 state transfers are observed over a time of 100 ms with hardly any decrease in fringe amplitude. Also, for measurements with $\tau_\pi=34.3$ μs, a fringe amplitude A close to unity has been observed for more than 150 state transfers. In both cases, the subsequent decay of the fringe amplitude for more oscillations indicates a limitation due to small fluctuations of the microwave power.

Unfortunately, microwave excitation does not couple motional and electronic states unless strong magnetic field gradients are applied [19] and it cannot be focused to a single qubit location. Nevertheless, microwave excitation turns out to be a useful reference for investigating the phase stability of Raman excitation schemes to be discussed in the next subsection.

B. Raman light field

In contrast to the microwave drive, the interaction region of the Raman field detuned from the dipole transition $S_{1/2}\leftrightarrow P_{1/2}$ is as small as the diameter of the involved laser beams. When a single ion is illuminated, the coupling to the center-of-mass mode along the trap axis (unit vector $\boldsymbol{e}_z$) is described by the Lamb-Dicke parameter $\eta=(\boldsymbol{k}_+ -\boldsymbol{k}_-)\cdot\boldsymbol{e}_z\sqrt{\frac{\hbar}{2M\omega}}$. Here, $\boldsymbol{k}_\pm$ is the wave vector of the blue and red Raman light fields, respectively, M is the mass of all ions in the string, and ω denotes the trap frequency. For copropagating lasers the Lamb-Dicke factor is negligible, whereas it is maximized for lasers counterpropagating along the motional mode axis.

We characterize the Raman interaction on a single ion by driving Rabi oscillations on the hyperfine qubit with copropagating beams from NW that are detuned from the $S_{1/2}$ to $P_{1/2}$ transition frequency by -10 GHz. Figure 7 shows Rabi oscillations for excitation times of up to 4 ms with a duration of a π pulse of $\tau_\pi=65.3(1)$ μs. The first few oscillations have a fringe amplitude of $A=0.97(1)$, which is reduced to 0.80(2) after more than 50 state transfers. Shot-to-shot variations in Raman light intensity contribute to a loss symmetrically to the average excitation. In addition, the fringe center, ideally at $y_0=0.5$, has dropped to $y_0=0.428(7)$ due to nonresonant scattering introduced by the Raman light field.

The ability to couple electronic and motional states by the Raman excitation was tested by comparing Rabi frequencies on the carrier and on the first blue sideband with noncopropagating beams (from NW and NE) illuminating an ion initially prepared in the motional ground state. The two Raman beams enclose a 90° angle such that the residual momentum transfer is optimized for the axial direction. From the ratio of the Rabi frequencies, we directly infer the Lamb-Dicke parameter to be $\eta=0.216(2)$, in good agreement with the theory.

VI. COHERENCE PROPERTIES OF THE $^{43}Ca^{+}$ HYPERFINE QUBIT

Applying the methods described before, we investigated quantum-information storage capabilities of the $^{43}Ca^{+}$ hyper-

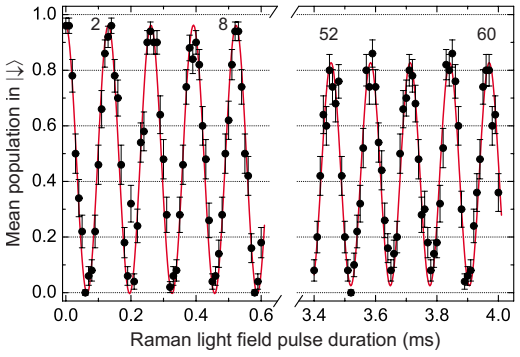

FIG. 7. (Color online) Rabi oscillations on the $^{43}Ca^{+}$ hyperfine qubit induced by a colinear Raman light field. Each data point represents 50 individual measurements. As for the microwave excitation, we fitted a sinusoidal function to the data set from 0 to 600 μs, which yields a fringe amplitude $A=0.97(1)$, a π time of $\tau_\pi=65.3(1)$ μs, and a fringe center at $y_0=0.479(5)$. Fitting to the data points beyond 3.4 ms, a small offset phase had to be introduced and τ_π adjusted to 63.8(2) μs, indicating a small increase of the Raman light power during the measurement. The amplitude reduced to $A=0.80(2)$, and the fringe center dropped to $y_0=0.428(7)$. A comparison with microwave excitation reveals imperfections caused by spontaneous scattering and laser amplitude fluctuations.

fine qubit. Limitations on the coherence time arise from both spontaneous scattering events and dephasing [16]. For the hyperfine qubit, spontaneous decay is negligible since the lifetime of the involved states can be considered as infinite for all practical purposes. Scattering can be induced though by imperfectly switched off laser beams. To judge the importance of this effect, we prepared the ion in the $|\downarrow\rangle$ state. After waiting for a time τ_d, we transferred the population with two subsequent π pulses to $D_{5/2}(F=6, m_F=0)$ and $D_{5/2}(F=4, m_F=2)$. Ideally no fluorescence should be observed. Figure 8 shows how an initial $|\downarrow\rangle$ population of 0.97 decreases with increasing waiting time τ_d. An exponential decay fit yields a time constant of 410 ms. This observation can be explained by imperfectly switching off the cooling laser at a wavelength of 397 nm by one single-pass AOM only. For every blue photon that is scattered, the ion will be lost from the state $|\downarrow\rangle$ with a high probability by decaying to one of the other $S_{1/2}$ Zeeman states. This complication was avoided by using a mechanical shutter completely switching off the Doppler cooling laser in all Rabi and Ramsey experiments lasting for 50 ms and longer.

Decoherence due to dephasing does not alter the state occupation probabilities. Instead, the phase information between driving field and the qubit gets lost. A powerful method to characterize this effect consists in measuring fringe amplitude in Ramsey phase experiments. Here a superposition of the two qubit states is created by a $\pi/2$ pulse. After a waiting time τ_R, during which the qubit evolves freely, a second $\pi/2$ pulse is applied. By scanning the Ramsey phase ϕ of the second pulse, a sinusoidal fringe pattern is observed whose fringe amplitude is a measure of the coherence.

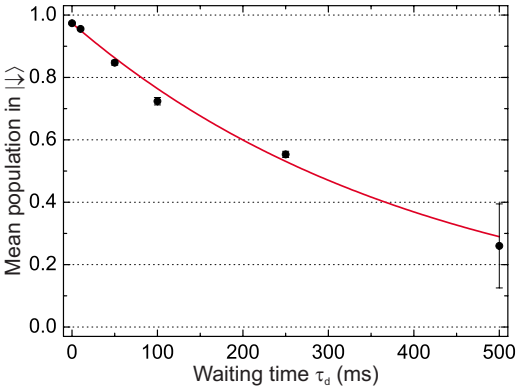

FIG. 8. (Color online) Measurement of the qubit state $|\downarrow\rangle$-population probability after a waiting time τ_d. Single-photon scattering events induced by residual light at 397 nm lead to a transfer of population from the $|\downarrow\rangle$ state to other Zeeman states in the ground-state manifold. The solid line is an exponential fit with a decay time constant of 410 ms.

For the Raman light field, the relevant phase is not only determined by the radio frequency devices supplying the AOMs creating the 3.2 GHz splitting, but also by the relative optical path length of the red and blue beamlines. In general, the absolute phase is not of interest as long as it does not change during the experiment. The setup can be considered as an interferometer whose sensitivity is also dependent on its size. In case of a copropagating Raman light field, the two beamlines are recombined on a polarizing beam splitter directly after the relative frequency generation. Here the interferometer encloses an area of about 0.04 m^2, whereas the

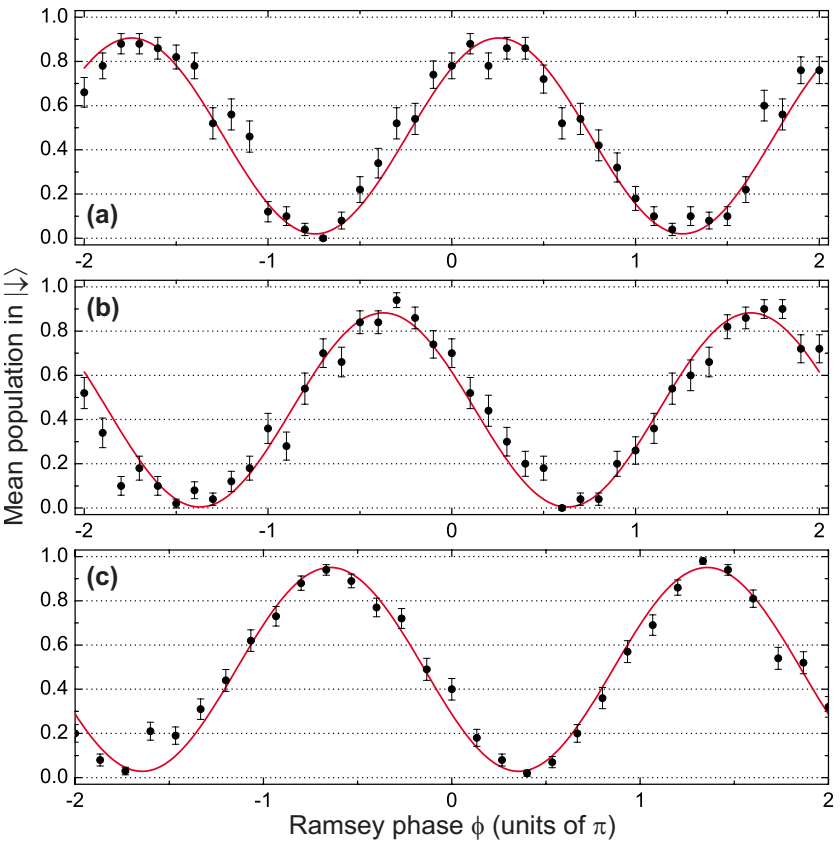

FIG. 9. (Color online) Ramsey phase experiments on the $^{43}Ca^+$ hyperfine qubit at a magnetic field of 3.4 G with a Ramsey waiting time τ_R set to 100 ms. The data were taken with three different driving fields. (a) Microwave drive with $\tau_\pi=19$ μs, (b) copropagating Raman light field with $\tau_\pi=20$ μs, and (c) noncopropagating Raman light field where $\tau_\pi=23$ μs. The fringe amplitudes are determined by weighted least-squares sinusoidal fits with amplitude A, offset phase Φ_0, and fringe center y_0 as free parameters. This yields fringe amplitudes of 0.886(17), 0.879(16), and 0.922(13), respectively. Dephasing by interferometric instabilities does not limit the experiments on these time scales. For Ramsey times beyond 100 ms, we observed a further decay of the fringe amplitude.

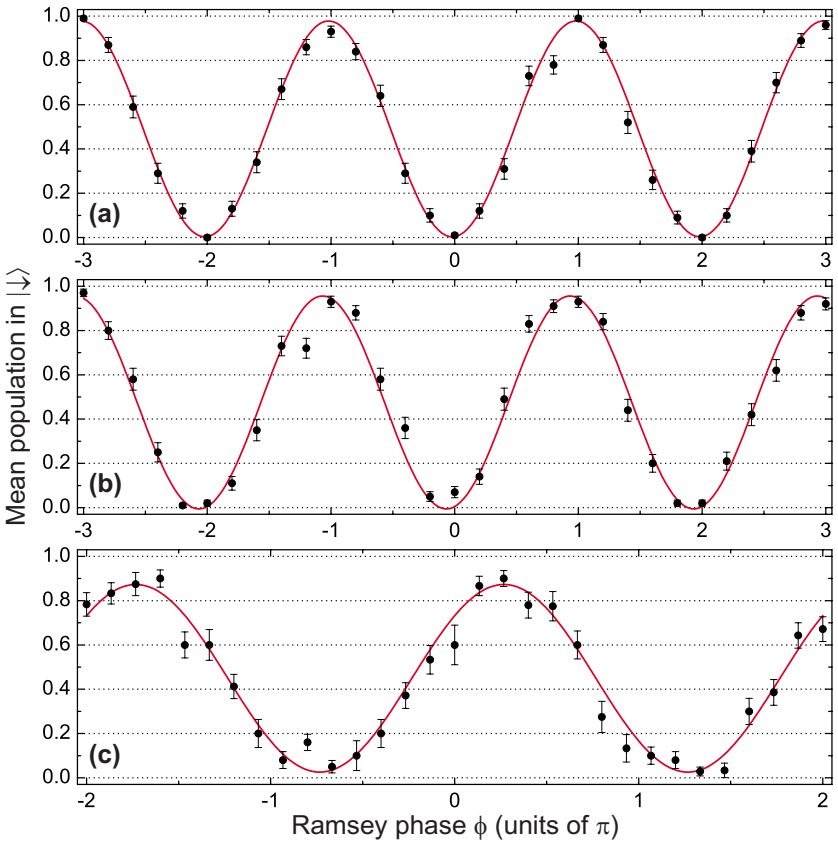

FIG. 10. (Color online) Ramsey phase experiments on the $^{43}Ca^{+}$ hyperfine qubit with microwave excitation at a magnetic field of 0.5 G. (a) A scan with $\tau_R = 50$ μs results an amplitude of 0.976(4) and demonstrates the ability of state initialization, manipulation, and readout. (b) For a Ramsey time $\tau_R = 200$ ms, the amplitude is 0.962(11). (c) For a Ramsey time of $\tau_R = 1$ s, a fringe amplitude of 0.847(21) was measured. Here the measurement time was about 90 min. The reduction of the amplitude is attributed to the residual sensitivity of 1.2 Hz/mG to ambient magnetic field fluctuations.

noncopropagating beams enclosing an area of about 0.15 m^2. In order to see whether the experiment would be limited by this effect, we investigated three different configurations.

Figure 9 shows the resulting Ramsey fringe patterns when driving the hyperfine qubit with (a) a microwave, (b) a copropagating Raman field, and (c) a noncopropagating Raman field. The Ramsey waiting time τ_R was set to 100 ms, the $\pi/2$ pulses having a duration of about 20 μs. Each data point represents either 50 or 100 measurements. The error bars indicate statistical errors and are used as weights when fitting the function $f(\phi) = \frac{A}{2}\sin(\phi + \phi_0) + y_0$ to the data in order to determine the fringe amplitude A. The parameters y_0 and ϕ_0 are also free fit parameters, but are not further considered. For the different excitation schemes, we find fringe amplitudes of 0.886(17), 0.879(16), and 0.922(13), respectively. From this we conclude that errors introduced by interferometric instabilities in generating the Raman beams do not limit our experiment on time scales up to 100 ms. For longer Ramsey times, we observed a further decay of fringe amplitude, which we attribute to dephasing. These measurements were performed at a magnetic field of 3.4 G. For small magnetic fields, the residual qubit sensitivity to magnetic field fluctuations increases linearly with a slope of 2.4 kHz/G^2. Therefore we reduced the magnetic field to 0.5 G and repeated the measurement with the microwave field. The resulting fringe patterns for three different Ramsey times τ_R are depicted in Fig. 10. A short waiting time of $\tau_R = 50$ μs results in a fringe pattern amplitude of (a) 0.976(4). This demonstrates the ability of reliable state initialization, readout, and single-qubit gate operation for the $^{43}Ca^{+}$ hyperfine qubit at low magnetic fields. For a Ramsey time of $\tau_R = 200$ ms we still obtain a fringe amplitude of (b) 0.962(11). A drop in amplitude to (c) 0.847(21) is observed only after increasing the Ramsey waiting time to $\tau_R = 1$ s.

Typically, the coherence time is defined as the Ramsey time for which the fringe amplitude A has dropped to a value of $1/e$. Extrapolation of our measurements would lead to a coherence time on the order of about 6.0 s assuming an exponential decay and 2.5 s for Gaussian decay. Comparing the measurements at 3.4 G and 0.5 G, we conclude that the main limitation to the coherence time comes from the residual sensitivity of the qubit at finite fields. Further improvements can be made by means of active magnetic field stabilization and passive shielding. In addition, rephasing can be achieved by an intermediate spin-echo pulse that exchanges the populations of the two qubit levels.

VII. SUMMARY AND DISCUSSION

In conclusion, we have discussed and demonstrated various experimental techniques for high-fidelity QIP with $^{43}Ca^{+}$ ions. These techniques were applied for measuring the quantum-information storage capabilities of the hyperfine qubit in a noisy environment to be many seconds. Furthermore, we demonstrated that interferometric instabilities due to Raman frequency creation do not limit the phase coherence on time scales up to 100 ms. For most experimental steps, use of the quadrupole transition laser is crucial for our scheme. It seems straightforward to apply these techniques to strings of ions without compromising the error rate. From other experiments with $^{40}Ca^{+}$ ions, we already have experi-

mental evidence that high-fidelity two-qubit operations are possible for the optical qubits [20]. It will be interesting to explore how these can be combined with the long storage times found here by swapping quantum information between hyperfine and optical qubits.

ACKNOWLEDGMENTS

We gratefully acknowledge the support of the European network SCALA, the Institut für Quanteninformation GmbH, DTO, and IARPA.

[1] J. I. Cirac and P. Zoller, Phys. Rev. Lett. **74**, 4091 (1995).
[2] D. Leibfried, R. Blatt, C. Monroe, and D. Wineland, Rev. Mod. Phys. **75**, 281 (2003).
[3] D. Leibfried, E. Knill, S. Seidelin, J. Britton, R. B. Blakestad, J. Chiaverini, D. B. Hume, W. M. Itano, J. D. Jost, C. Langer *et al.*, Nature (London) **438**, 639 (2005).
[4] K.-A. Brickman, P. C. Haljan, P. J. Lee, M. Acton, L. Deslauriers, and C. Monroe, Phys. Rev. A **72**, 050306(R) (2005).
[5] P. C. Haljan, P. J. Lee, K.-A. Brickman, M. Acton, L. Deslauriers, and C. Monroe, Phys. Rev. A **72**, 062316 (2005).
[6] F. Schmidt-Kaler, H. Häffner, M. Riebe, S. Gulde, G. P. T. Lancaster, T. Deuschle, C. Becher, C. F. Roos, J. Eschner, and R. Blatt, Nature (London) **422**, 408 (2003).
[7] M. Riebe, H. Häffner, C. F. Roos, W. Hänsel, J. Benhelm, G. P. T. Lancaster, T. W. Körber, C. Becher, F. Schmidt-Kaler, D. F. V. James *et al.*, Nature (London) **429**, 734 (2004).
[8] H. Häffner, W. Hänsel, C. F. Roos, J. Benhelm, D. C. al Kar, M. Chwalla, T. Körber, U. D. Rapol, M. Riebe, P. O. Schmidt *et al.*, Nature (London) **438**, 643 (2005).
[9] L. Aolita, K. Kim, J. Benhelm, C. F. Roos, and H. Häffner, Phys. Rev. A **76**, 040303(R) (2007).
[10] F. Arbes, M. Benzing, T. Gudjons, F. Kurth, and G. Werth, Z. Phys. D: At., Mol. Clusters **31**, 27 (1994).
[11] J. Benhelm, G. Kirchmair, U. Rapol, T. Körber, C. F. Roos, and R. Blatt, Phys. Rev. A **75**, 032506 (2007).
[12] S. Gulde, D. Rotter, P. Barton, F. Schmidt-Kaler, R. Blatt, and W. Hogervorst, Appl. Phys. B: Lasers Opt. **73**, 861 (2001).
[13] D. M. Lucas, A. Ramos, J. P. Home, M. J. McDonnell, S. Nakayama, J. P. Stacey, S. C. Webster, D. N. Stacey, and A. M. Steane, Phys. Rev. A **69**, 012711 (2004).
[14] F. Schmidt-Kaler, H. Häffner, S. Gulde, M. Riebe, G. P. T. Lancaster, T. Deuschle, C. Becher, W. Hänsel, J. Eschner, C. F. Roos *et al.*, Appl. Phys. B: Lasers Opt. **77**, 789 (2003).
[15] M. Notcutt, L.-S. Ma, J. Ye, and J. L. Hall, Opt. Lett. **30**, 1815 (2005).
[16] D. M. Lucas, B. C. Keitch, J. P. Home, G. Imreh, M. J. McDonnell, D. N. Stacey, D. J. Szwer, and A. M. Steane, e-print arXiv:0710.4421.
[17] C. Roos, T. Zeiger, H. Rohde, H. C. Nägerl, J. Eschner, D. Leibfried, F. Schmidt-Kaler, and R. Blatt, Phys. Rev. Lett. **83**, 4713 (1999).
[18] T. Lu, X. Miao, and H. Metcalf, Phys. Rev. A **71**, 061405(R) (2005).
[19] F. Mintert and C. Wunderlich, Phys. Rev. Lett. **87**, 257904 (2001).
[20] J. Benhelm, G. Kirchmair, C. F. Roos, and R. Blatt, Nat. Phys. **4**, 463 (2008).
[21] H.G. Dehmelt, Bull. Am. Phys. Soc. **20**, 60 (1975).